Crimson Publishers
Wings to the Research

Mini Review

Characterization of the Hoidas Lake Rare Earth Deposit

Corby G Anderson*

Kroll Institute for Extractive Metallurgy, Colorado School of Mines, USA

ISSN: 2578-0255

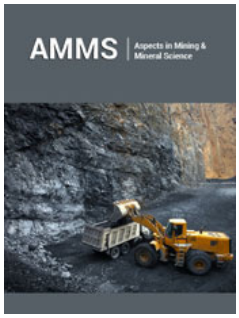

***Corresponding author:** Corby G Anderson, Kroll Institute for Extractive Metallurgy, Colorado School of Mines, Golden, Colorado, USA

Submission: September 28, 2022

Published: October 28, 2022

Volume 10 - Issue 2

How to cite this article: Corby G Anderson*. Characterization of the Hoidas Lake Rare Earth Deposit. Aspects Min Miner Sci. 10(2). AMMS. 000731. 2022. DOI: 10.31031/AMMS.2022.10.000731

Abstract

Hoidas Lake lies in the Northern Rae Geological Province, in the general vicinity of many of Saskatchewan's large uranium mines. The mineralogy of the Hoidas Lake rare-earth deposit differs from most other such deposits in that it is hosted in equal abundance in veins containing apatite and allanite mineral groups. Hoidas Lake also differs from other deposits in that it contains a significant amount of heavy rare-earth elements, such as dysprosium [1-5]. This abundance of heavy Rare Earth Elements (REE's) is significant, as there is a growing demand for the heavier rare earths in high-tech manufacturing (such as the use of dysprosium in the manufacturing of hybrid car components).

Keywords: Hoidas lake; Rare earth elements; Characterization

Introduction

Research was provided for assessing ten (10) boxes of core samples provided by Great Western Minerals. This provided a basis for further metallurgical testing which included beneficiation and hydrometallurgical rare earth separation and recovery [6-12]. The following work was done on the ten (10) core samples;

a. Core and bulk composite ore preparation

b. Mineralogical examinations

c. X-Ray diffraction

d. ICP elemental analysis

e. Sulfur and carbon analysis

f. SEM/EDX analysis

g. Abrasion indices of a bulk blended composite sample

h. Bond grindability index of bulk bended composite sample

i. Reporting

Mineralogical Examinations

Ten specimens from the boxed core were selected for thin sections. An effort was made to obtain a representative suite of the various lithologies represented by this core. Preliminary petrographic examination was made of these thin sections accompanied by SEM and EDX analyses of some specimens. The following observations are the most important ones to be considered in carrying out subsequent beneficiation tests on these cores [13-20].

a. The report done by the Mineral Exploration Branch of the Saskatchewan Research Council is excellent. They did a very detailed and accurate petrographic analysis of their specimens. These descriptions together with their chemical analyses are a good starting point for beneficiation tests on the cores.

b. Apart from ilmenite and scapolite we observed all of the minerals described in their report. The carbonate that they described is calcite.

c. Several of the specimens are strongly altered presumably by hydrothermal solutions. Minerals that are specifically altered are plagioclase to a fine-grained mineral, perhaps sericite; biotite to chlorite; and hornblende to what is probably a mixture of fine-grained epidote and chlorite. The K-feldspar is generally unaltered.

d. Apatite is a major constituent of two specimens (HL -1 IB and HL - 13B).

e. HL10-B contains a fine-grained unidentified yellowish mineral that forms veinlets and a chalcedony vein let.

f. None of these specimens has a high concentration of allanite. The mineral marked in HL13-A will be checked by EDX. It looks like titanite and doesn't fit the description of allanite in the report.

g. Specimen HL-13B consists mainly of apatite with small grains of metamict allanite with radiating fractures.

Then individual thin section analysis was as follows.

i. **HL 5A:** Partly altered quartzofeldspathic gneiss that consists of quartz, K-feldspar, partly altered (sericitized?) plagioclase, hornblende, and partly chloritized biotite.

ii. **HL 5B:** Sheared quartzofeldspathic gneiss or granite that consists of quartz, K-feldspar, partly altered plagioclase, hornblende and chlorite.

iii. **HL 10A:** Quartzofeldspathic gneiss with quartz, K-feldspar, slightly altered plagioclase, partly chloritized biotite (accompanied by titanite), diopside, and rare apatite.

iv. **HL 10B:** Quartzofeldspathic gneiss that consists of quartz, K-spar, plagioclase, hornblende, and minor titanite. Veinlets of fine-grained layer silicate and chalcedony.

v. **HL 10C:** This specimen consists minimally of K-feldpsar and hornblende with lesser biotite. Biotite is partly chloritized and hornblende is partly altered to epidote. Titanite and apatite are minor constituents.

vi. **HL 10D:** This cataclasite consists of K-feldspar, altered hornblende, and apatite. A fine-grained layer silicate surrounds K-feldspar and apatite clasts. Allanite was tentatively identified by EDX. Calcite is a trace constituent.

vii. **HL 11A:** This specimen consists of quartz, K-feldspar, plagioclase, hornblende, and minor apatite. Titanite is a trace constituent.

viii. **HL 11B:** This cataclasite consists of quartz, K-feldspar, plagioclase, hornblende, and apatite. EDX shows Ba in the K-feldspar indicating that it is hyalophane. Allanite was tentatively identified by EDX. A fine-grained layer silicate surrounds many of the clasts.

ix. **HL 13A:** This specimen consists of quartz, K-feldspar, diopside, and minor apatite and titanite.

x. **HL 13B:** This specimen consists mainly of apatite and minor hornblende. The tan, isotropic grains in apatite are tentatively identified to be metamict allanite. Thorite was tentatively identified by EDX. Calcite is a trace constituent.

An example pictures from the mineralogical thin section analysis of sample #1 is illustrated in Figure 1. ICP

Figure 1: Core thin section image example.

ICP Elemental Scans of Core and Composites Samples

ICP elemental scans were performed for all core samples and the composite and the pertinent analysis for each expressed in ppm follows (Figure 2).

Sample #1 HL 10 BX 10 43-2 – 47-4

Sample #2 HL 10 BX 10 39.2-43.2

Sample #3 HL 11 BX 11 44.5-48.7

Sample #4 HL 13 BX 8 34.75 – 39.0

Sample #5 HL 10 BX 12 47.0 – 51.7

Sample #6 HL 5 BX 7 26.7-32.3

Sample #7 HL 10 BX 13 51.7-56

Sample #8 HL 5 BX 8 32.3-36.6

Sample #9 HL 13 BX 9 39.2 – 43.5

Sample #10 HL 11 BX 10 43.3 – 44.5

Sample #11 Composite sample

Sample	#1	#2	#3	#4	#5	#6	#7	#8	#9	#10	#11	#1 rpt
Ag 328.068	-1	3	1	6	0	0	1	0	2	8	2	0
Al 237.313	31300	50500	34200	21700	46000	46200	61110	31600	36400	18400	125	30300
As 188.980	18	10	23	33	11	15	3	0	5	6	616	15
Au 197.742	0	0	0	0	0	0	0	1	0	5	14	0
B 249.677	63	874	656	697	633	673	505	779	1010	890	2710	78
Ba 233.527	15300	8990	10400	9400	12000	3080	1320	1310	5050	1560	17	15300
Be 313.107	4.2	2.9	3.2	1.8	2.7	1.6	1.3	0.8	2.3	0.7	0.1	4.2
Bi 223.061	4	0	0	0	1	0	-1	0	1	1	20	0
C 193.027	2810	4640	2510	3250	3330	7290	5440	797	5110	2000	5390	4260
Ca 300.686	135000	118000	195000	245000	108000	95400	25600	15900	67100	14100	695	132000
Cd 228.802	0.7	0.4	0.3	0.6	0.4	0.5	0.3	0.1	0.4	0.4	32.3	0.3
Ce 418.659	4130	2450	4350	6900	1990	2860	199	442	1390	350	11	4110
Co 228.616	1	4	1	11	2	3	-1	-4	3	-5	-9	1
Cr 267.716	445	374	143	289	557	158	206	301	259	118	432	275
Cs 459.311	-9200	-6930	-8470	-10400	301	-4650	-5140	-5230	-6060	-5140	12000	-9620
Cu 327.395	87	123	138	205	93	159	79	124	113	173	303	79
Dy 340.780	58	31	68	92	28	38	4	4	21	4	0	56
Er 369.265	11	6	13	16	8	7	2	1	5	2	16	10
Eu 412.964	66	33	77	105	30	43	2	4	15	4	0	65
Fe 218.719	30200	39600	27200	35100	34200	21800	18710	12700	19200	7470	-4870	29110
Ga 294.363	14	55	55	69	0	0	0	5	42	6	15	51
Gd 336.224	153	73	177	232	64	97	3	7	52	5	-1	151
Ge 269.134	1	23	8	54	32	17	15	133	13	15	17	3

Sample	#1	#2	#3	#4	#5	#6	#7	#8	#9	#10	#11	#1 rpt
Hf 196.361	1	0	1	0	1	1	3	2	0	3	2	0
Hg 184.888	4	3	3	3	2	2	2	2	3	1	50	3
Ho 345.600	12	13	16	18	14	14	9	6	7	3	0	12
I 182.976	100	3050	2250	1560	1290	1320	1400	1860	234	79	7	14
In 230.606	17	2	3	3	2	4	2	1	2	0	14	5
K 769.897	51400	85600	74700	41100	94500	96400	82000	58400	43000	27600	11000	50800
La 333.749	1730	1070	1810	3260	934	1370	101	244	629	176	3	1720
Li 610.358	12	8	5	4	11	5	3	1	0	73	0	11
Lu 291.139	1	0	1	2	0	0	0	0	0	0	0	1
Mg 182.731	36700	27200	30700	21300	31800	5210	11400	5920	12600	5400	188	35300
Mn 257.610	496	725	467	397	708	224	174	115	367	122	-72	473
Mo 202.032	2	3	0	17	9	10	2	2	7	55	103	-1
Nb 295.088	0	1	0	0	3	0	4	1	2	1	1	0
Nd 390.587	2680	1490	2910	4300	1270	1800	123	243	901	186	46	2650
Ni 231.604	192	246	190	326	196	207	197	139	246	66	46	267
Os 228.227	<5	<5	<5	<5	<5	<5	<5	<5	<5	<5	<5	<5
P 178.703	41100	24600	60800	77600	20400	31000	2900	2730	20100	4300	9610	40000
Pb 220.354	318	192	282	87	58	59	241	26	107	25	372	275
Pd 351.694	<5	<5	<5	<5	<5	<5	<5	<5	<5	<5	<5	<5
Pr 422.294	518	280	555	846	236	352	12	43	149	32	3	502
Pt 214.424	<5	<5	<5	<5	<5	<5	<5	<5	<5	<5	<5	<5
Rb 780.026	50	98	81	39	111	136	111	72	81	21	7	48
Re 197.248	1	2	0	0	1	0	3	3	0	2	17	2
Rh 343.488	<5	<5	<5	<5	<5	<5	<5	<5	<5	<5	<5	<5

Sample	#1	#2	#3	#4	#5	#6	#7	#8	#9	#10	#11	#1 rpt
Ru 210.734	<5	<5	<5	<5	<5	<5	<5	<5	<5	<5	<5	<5
S 181.972	5230	6160	3380	0	2570	1580	676	541	4060	3260	205000	5600
Sb 217.582	2	0	0	0	0	0	11	0	0	1	9	0
Sc 357.634	8	8	8	9	7	3	4	2	6	2	0	8
Se 196.026	9	2	-3	6	2	1	-3	0	0	7	1220	7
Si 251.611	604000	173000	123000	79500	151000	191000	188000	124000	159000	50700	803	233000
Sm 359.259	341	172	388	547	150	211	9	17	97	14	0	336
Sn 189.927	41	55	48	48	41	44	45	26	46	15	4	47
Sr 460.733	6770	5790	11000	0	6100	3030	891	637	8090	1920	27	6720
Ta 205.908	21	13	32	19	14	19	53	9	30	19	16	29
Tb 357.920	20	11	24	32	9	13	1	1	7	2	0	20
Te 214.282	16	3	13	30	-1	7	-8	-6	6	-4	10	13
Th 259.705	359	160	314	497	130	234	10	26	120	13	6	332
Ti 334.940	1060	1380	1340	1280	1030	894	1370	816	1260	668	1	1070
Tl 190.794	1	-1	0	0	0	0	1	1	0	2	30	0
Tm 313.125	0.36	0.04	0.48	1.31	0	0	0	0	0	0	1.15	0.43
U 409.013	11	5	10	16	6	7	0	2	3	1	3	11
V 292.402	36	46	37	35	33	23	27	14	33	12	3	36
W 207.121	0	5	3	0	4	0	2	0	0	1	3	0
Y 371.028	189	94	222	287	85	125	14	13	74	11	1	186
Yb 218.572	8.13	4.67	9.59	12	4.22	5.38	1.23	0.9	3.72	0.85	0	8.25
Zn 334.502	107	113	113	98	87	43	32	56	79	45	96	101

Figure 2: ICP elemental scans were performed for all core samples and the composite.

Sample Carbon and Sulfur Analysis

Sulfur and carbon analysis of each core sample and composite was performed. The results are as follows (Table 1).

Table 1: Sulfur and carbon analysis of core sample and composite.

Sample ID			
Box #	**Depth**	**Carbon (%)**	**Sulfur (%)**
HL 5 BX 7	26.7-32.3	0.29	0.13
HL 5 BX 8	32.3-36.6	0.2	0.06
HL 10 BX 10	39.2-43.2	0.65	0.53
HL 10 BX 10	43.2-47.4	0.78	0.65
HL 10 BX 12	47.0-51.7	1.36	0.28
HL 10 BX 13	51.7-56	0.12	0.05
HL 11 BX 10	40.3-44.5	0.4	0.52
HL 11 BX 11	44.5-48.7	0.41	0.34
HL 13 BX 8	34.75-39	0.51	1.53
HL 13 BX 9	39.2-43.5	0.23	0.5
Composite	All	0.37	0.37

SEM EDX Analysis

Scanning electron microscopy along with energy dispersive x-ray analysis was undertaken on the thin section samples which had been prepared for the thin section analysis. A summary follows. Thin sections, mounted on glass microscope slides, Were commercially prepared. Then examinations, were carried out on the sections with a petrographic microscope [21-30]. A few areas on a few of the slides Were marked as worth examination by SEM/EDX in order to get some chemical identification of the mineral materials. The SEM/EDX equipment used comprised a LEO 1430VP SEM (operated with a tungsten source), and a PGT Sahara silicon drift detector (LN2-free, resolution about 140ev FWHM at Mn Ka, with detection down to carbon), and the PGT Spirit software suite. The SEM was operated at 20kv with a chamber pressure of 15Pa, so that no coating of the sections was necessary. A quad back scatter detector in the compositional mode was used to image the specimens. This means the contrast in the images was almost entirely due to average atomic number variations.

The general approach was to locate any areas previously marked and to obtain x-ray spectra from various spots within the marked areas. This was mostly done by so-called Spotlight analysis which involves tagging the SEM images at places of interest using the SEM external scan control to then collect automatically an x-ray spectrum from each tagged spot for some period, usually 80 or 100 seconds. The data accompanying this report thus consists of several BSE images showing numbered tagged areas along with the x-ray spectrums from these tagged spots [31-35]. A standardless quantitative analysis was performed on each spot and the result, expressed as elemental and as oxygen compound per cent, is given for each spectrum. It is noted that a carbon peak of some degree was usually present, but carbon was not included in the list of analyzed elements mostly because it was suspected that the carbon came from the cement used to adhere the sections to the glass slides. Aside from the areas marked the sections Were also traversed under the electron beam seeking bright (i.e. metal rich) areas or other features deemed interesting. In the interest of time and expense this search was mostly done at a magnification of lOOX and this means that only a fraction of the total area on a slide was scrutinized in this way. For the most part there were

few significant areas containing thorium except for the monazite crystals circled. Rare earth metals were identified as present in all the sections but generally in very small areas. The mineralization is evidently quite complex and zircon crystals were found, occasional pyrite, a strontium mineral, titanium mineral, and barite. The rocks generally were apatite, quartz, and feldspar. We were informed that Scandium at the 2-3gm/t level had been reported in these samples. The encyclopedia states that Scandium is found associated with rare earth elements. This level is essentially below the detectability limit for EDX but even when the electron beam spot is positioned on a rare earth mineral (presumably elevating the Scandium level closer to detectability) the Scandium Ka peak at 4.091kev is located so close to the Calcium KB line at 4.012kev that the overlap renders trace quantities of Scandium invisible. To compound the problem there is a lesser Lanthanum peak even closer to the Scandium peak so that the overlap problem is very formidable [36-41].

X-Ray Diffraction Analysis

X-ray diffraction analysis was also undertaken on the samples. Again, the description, major phases found, and sample numbering was as follows.

Sample #1 HL 10 BX 10 43-2 – 47-4 albite, quartz, fluorapatite, lazulite.

Sample #2 HL 10 BX 10 39.2-43.2 fluorapatite, hydroxylapatite, orthoclase, microline, hyalophane.

Sample #3 HL 11 BX 11 44.5-48.7 fluorapatite, britholite, microperthite, potassium feldspar, orthoclase.

Sample #4 HL 13 BX 8 34.75 – 39.0 microperthite, potassium feldspar, orthoclase, quartz, calcite.

Sample #5 HL 10 BX 12 47.0 – 51.7 quartz, albite, microcline, potassium feldspar.

Sample #6 HL 5 BX 7 26.7-32.3 quartz, potassium feldspar, microcline, albite, fluorapatite.

Sample #7 HL 10 BX 13 51.7-56 fluorapatite, hydroxylapatite, potassium feldspar.

Sample #8 HL 5 BX 8 32.3-36.6 quartz, potassium feldspar, albite, microperthite, fluorapatite.

Sample #9 HL 13 BX 9 39.2 – 43.5 potassium feldspar, orthoclase, microperthit, microcline, albite.

Sample #10 HL 11 BX 10 43.3 – 44.5 quartz, albite, microcline, potassium feldspar.

Sample #11 Composite sample Quartz, albite, microcline.

Bond Grindability of Bulk Blended Composite Sample

The weighted composite sample was tested by conventional Bond work index grindability testing. The work index was found to be 5.72KwHr/ton.

Relative Abrasion Index

Based on the estimated silica content of the composite sample, the relative abrasion index is estimated to be about 0.25lb. of metal per kw-hr of energy used in crushing or grinding.

Summary

Ten boxes of core samples from the Hoidas Lake rare earth deposit were received. Fundamental mineralogical and metallurgical characterizations were carried out on these samples in preparation of beneficiation and hydrometallurgical testing. No mineralogical anomalies surprises were found, and the material appeared representative for subsequent metallurgical testing and process development.

Acknowledgement

Thank you to Dr. Richard Berg of the Montana Bureau of Mines and Geology for his insights and efforts on the SEM EDX research.

References

1. Pandur K, Ansdell KM, Kontak DJ, Halpin KM, Creighton S (2016) Petrographic and mineral chemical characteristics of the Hoidas Lake Deposit, Northern Saskatchewan, Canada: Constraints on the origin of a distal magmatic-hydrothermal REE system. Economic Geology 111(3): 667-694.
2. U S Department of the Interior, U S Geological Survey, Critical Mineral Resources of the United States-Economic and Environmental Geology and Prospects for Future Supply. In: Schulz KJ, DeYoung JH, Seal RR, Bradley DC (2018) Professional Paper 1802.
3. Keller P, Anderson CG (2018) The production of critical materials as by products. Aspects in Mining and Mineral Science 2(2): 208-221.
4. Keller P, Anderson CG (2018) Co production of critical energy materials. Research and Development in Materials Science 4(4): 382-383.
5. Anderson CG (2016) Industrial manufacture of by product critical materials. Presented at the DOE CMI Annual Meeting.
6. Anderson CG (2016) The critical aspect of critical materials. Presented at the DOE CMI Webinar Series.
7. Eggert R, Wadia C, Anderson CG, Bauer D, Fields F, et al. (2016) Rare earths: Market disruption, innovation, and global supply chains. Annual Review of Environment and Resources 41: 199-222.
8. Imholte D, Nguyen R, Vedantam A, Brown M, Iyer A, et al. (2017) An assessment of U.S. rare earth availability for supporting U.S. wind energy growth targets. Energy Policy 113: 294-305.
9. Anderson CD, Taylor P, Anderson CG (2017) Rare earth flotation fundamentals: A review. American Journal of Engineering Research 6(12): 155-166.
10. Anderson CD, Taylor P, Anderson CG (2016) Rare earth flotation fundamentals: A review. IMPC 2016 Proceedings of the XXVIII International Mineral Processing Congress.
11. Anderson CD (2015) Improved understanding of rare earth surface chemistry and its application to froth flotation. KIEM PhD thesis, Colorado School of Mines, USA.
12. Kronholm B, Anderson C, Taylor P (2013) A primer on hydrometallurgical rare earth separations. Journal of Metals 65: 1321-1326.
13. Kronholm B, Anderson CG (2020) Upgrade of Yttrium in a mixed rare earth stream using iminodiacetic acid functionalized resin. U S Patent 10,696,562.

14. Kronholm B (2019) Upgrade of yttrium in a mixed rare earth stream using iminodiacetic acid functionalized resin. KIEM MSc thesis, Colorado School of Mines, USA.

15. Zhang Y, Gu F, Su Z, Liu S, Anderson C, et al. (2020) Hydrometallurgical recovery of rare earth elements from NdFeB permanent magnet scrap: A review. Metals 10(6): 841.

16. Schriner D, Anderson C (2015) Metallurgical evaluation of the Hoidas Lake rare earth deposit. Journal of Metallurgical Engineering 4: 69-77.

17. Schriner D (2015) Advanced beneficiation of bastnaesite ore through centrifugal concentration and froth flotation. KIEM MSc Thesis, Colorado School of Mines, USA.

18. Norgren C (2018) Physical beneficiation of bastnaesite. KIEM MSc Thesis, Colorado School of Mines, USA.

19. Everly D (2017) The evaluation of selective collectors for bastnaesite flotation. KIEM MSc Thesis, Colorado School of Mines, USA.

20. Everly D, Anderson CG, Jansone-Popova S, Bryantsev V, Moyer B (2020) Flotation of bastnaesite ore using novel collectors. Proceedings of CIM MetSoc Annual Meeting.

21. Williams N (2018) Bastnaesite beneficiation by froth flotation and gravity separation. KIEM MSc Thesis, Colorado School of Mines, USA.

22. Owens CL, Nash GR, Hadler K, Fitzpatrick RS, Anderson CG, et al. (2018) Zeta potentials of the rare earth element fluorcarbonate minerals focusing on bastnäsite and parasite. Advances in Colloid and Interface Science 256: 152-162.

23. Zhang Y, Anderson C (2016) Surface chemistry and microflotation of xenotime and selected gangue minerals using octanohydroxamic acid as the collector. Journal of Sustainable Metallurgy 3: 39-47.

24. Zhang Y, Anderson C (2016) A comparison of sodium silicate and ammonium lignosulfonate effects on xenotime and selected gangue mineral microflotation. Minerals Engineering 100: 1-8.

25. Zhang Y (2016) Froth flotation of xenotime. KIEM MSc Thesis, Colorado School of Mines, USA.

26. Mushidi J, Anderson C (2017) Surface chemistry and flotation behaviors of monazite–apatite–ilmenite–quartz–rutile–zircon with octanohydroxamic acid. Journal of Sustainable Metallurgy 3: 62-72.

27. Mushidi J (2016) Surface chemistry and flotation behavior of monazite, apatite, ilmenite, quartz, rutile, and zircon using octanohydroxamic acid collector. KIEM MSc Thesis, Colorado School of Mines, USA.

28. Cui H, Anderson C (2016) The simulation and preliminary studies on bear lodge ore flotation. Conference: SME Annual Meeting, At Phoenix, Arizona, Volume: Plant Design Session.

29. Cui H, Anderson C (2018) Part of the Minerals, Metals & Materials Series book series (MMMS), Extraction.

30. Cui H, Anderson C (2017) Alternative flowsheet for rare earth beneficiation of bear lodge ore. Minerals Engineering 110: 166-178.

31. Cui H, Anderson C (2017) Fundamental studies on the surface chemistry of ancylite, calcite, and strontianite. Journal of Sustainable Metallurgy 3: 48-61.

32. Cui H (2015) Beneficiation of rare earth element bearing ancylite. KIEM MSc Thesis, Colorado School of Mines, USA.

33. Cui H, Anderson C (2020) Beneficiation of ancylite. U S Patent 10,618,058.

34. Vaccarezza V, Anderson C (2018) Beneficiation and leaching study of Norra Karr eudialyte mineral. Proceedings of Rare Metals Technology 2018, TMS, 39-51.

35. Vaccarezza V (2017) Beneficiation and hydrometallurgical treatment of Norra Karr eudialyte material. KIEM MSc Thesis, Colorado School of Mines, USA.

36. Vaccarezza V, Anderson C (2020) An overview of beneficiation and hydrometallurgical techniques on eudialyte group minerals. Mining, Metallurgy and Exploration 37: 39-50.

37. Owens CL, Nash GR, Hadler K, Fitzpatrick RS, Anderson CG, et al. (2019) Apatite enrichment by rare earth elements: A review of the effects of surface properties. Advances in Colloid and Interface Science 265: 14-28.

38. Anderson CG, Miranda PJ (2020) Metallurgical evaluation of the Hoidas Lake rare earth deposit. Metallurgical and Materials Engineering 26(2): 143-162.

39. Norgren C, Anderson C (2021) Ultra-fine centrifugal concentration of bastnaesite ore. Metals 11(10).

40. Norgren C, Anderson C (2022) Recovery of rare earth oxides from flotation concentrates of bastnaesite ore by ultra-fine centrifugal concentration. Metals.

41. Colligan G, O Kelley B, Anderson C (2022) Novel methods for bastnaesite concentrate leaching. Mining Metallurgy & Exploration Journal 39: 31-38.